

Transverse Beam Dynamics including Aberration Effects in the Thermal Wave Model using a Functional Method

Ji-ho Jang¹, Yong-sub Cho, Hyeok-jung Kwon

Korea Atomic Energy Research Institute, Daejeon 305-353, Korea

We studied the transverse beam dynamics including aberration effects of sextupole and octupole perturbations in a thermal wave model. A functional integration method was used to calculate the first-order perturbation effects. We found that the model successfully explains a PARMILA simulation results for proton beams without space-charge effects in a FODO lattice.

Abstract

PACS: 29.27.-a, 29.27.Eg

Keywords: Transverse Beam Dynamics, Aberration, Thermal Wave Model, Functional Method

¹jangjh@kaeri.re.kr

The thermal wave model (TWM) can be used to study the beam dynamics for relativistic charged particles [1]. This model was used to estimate the luminosity for a beam perturbed by the spherical aberration in a linear collider [2] and explain the halo formation by using a Gaussian slit [3]. The transverse beam dynamics of charged particles is a promising branch of the TWM. In ref. [4], authors showed that the particle distribution was successfully described by the TWM in a thin lens approximation of a quadrupole magnet with aberration. It can be extended to a general quadrupole lattice for a Gaussian beam by using a functional integration method if the space charge effects can be neglected [5]. However the work was restricted to a perfect quadrupole magnet. In this paper, we extended the TWM formulation for a transverse beam dynamics to include a sextupole and an octupole perturbations by using the first-order perturbation theory of a functional method. The model calculation was compared to the PARMILA [6] simulation result in a FODO lattice. We found that the model can explain the PARMILA results successfully if the perturbation effect is not too large.

In TWM, the beam wave function of the relativistic charged particle can be described by the Schrödinger-type equation as following,

$$i \epsilon \frac{\partial \psi(x, z)}{\partial z} = - \frac{\epsilon^2}{2} \frac{\partial^2}{\partial x^2} \psi(x, z) + U(x, z) \psi(x, z), \quad (1)$$

where $z = ct$ is the longitudinal coordinate of the beam motion and $U(x, z) \equiv u(x, z)/m_0\gamma\beta^2c^2$ is the dimensionless potential. The transverse beam distribution function is given by a modulus squared of the beam wave function, $\rho(x, z) = N |\psi(x, z)|^2$ with a particle number of N . The beam wave function satisfies the following normalization condition, $\int_{-\infty}^{\infty} |\psi(x, z)|^2 dx = 1$.

The initial Gaussian beam wave function can be described by

$$\psi_1(x, 0) = \left(\frac{1}{2\pi\sigma_1^2} \right)^{\frac{1}{4}} \exp \left[-\frac{x^2}{4\sigma_1^2} + i \left(\frac{x^2}{2\epsilon\rho_1} + \theta_1 \right) \right]. \quad (2)$$

where $\epsilon = 2\epsilon_{\text{rms}}$ with the unnormalized rms emittance of ϵ_{rms} . The parameters, σ_1 and ρ_1 are related to the twiss parameters of the initial particle distribution through $\sigma_1 = \sqrt{\epsilon_{\text{rms}}\beta_1}$ and $\rho_1 = -\beta_1/\alpha_1$ [5]. An elegant way to solve the differential equation (Eq. (1)) is a functional integral method where the solution is given by the product of kernel (or propagator) and the initial beam wave function,

$$\psi(x_2, z) = \int_{-\infty}^{\infty} dx_1 K(x_2, z; x_1, 0) \psi(x_1, 0). \quad (3)$$

When we include the sextupole and octupole perturbation, the potential can be described as

$$V(x) = U_0(x) - U_p(x), \quad (4)$$

with

$$U_0(x) = \frac{k_2}{2}x^2, \quad U_p(x) = \frac{k_3}{3!}x^3 + \frac{k_4}{4!}x^4. \quad (5)$$

where $U_0(x)$ is the potential of a quadrupole magnet and $U_p(x)$ describes the aberration effects. The k_2 , k_3 , and k_4 are related to the field strength of the quadrupole, sextupole, and octupole magnets.

In the first-order perturbation, the kernels for a focusing and defocusing quadruple magnets become

$$K_f(x_2, z; x_1, 0; V_p(x)) = K_f^{(0)}(x_2, z; x_1, 0) \left(1 + \sum_{n=0}^4 h_n(x_2, z) \left(\frac{x_1}{\sigma_0} \right)^n \right), \quad (6)$$

$$K_d(x_2, z; x_1, 0; V_p(x)) = K_d^{(0)}(x_2, z; x_1, 0) \left(1 + \sum_{n=0}^4 g_n(x_2, z) \left(\frac{x_1}{\sigma_0} \right)^n \right). \quad (7)$$

where $K_f^{(0)}(x_2, z; x_1, 0)$ is the unperturbed kernel for a focusing case as given in Ref. [5]:

$$K_f^{(0)}(x_2, z; x_1, 0) = \left(\frac{\sqrt{k_1}}{2\pi i \epsilon \sin(\sqrt{k_1} z)} \right)^{1/2} e^{i \frac{\sqrt{k_1}}{2\epsilon} [(x_2^2 + x_1^2) \cot \sqrt{k_1} z - 2x_2 x_1 \csc \sqrt{k_1} z]} \quad (8)$$

The kernel $K_d^{(0)}$ for the defocusing case is obtained by replacing \cot and \csc functions in the focusing case with \coth and csch functions, respectively. From the functional perturbation theory [7], we obtained the coefficient functions for a focusing quadrupole as follows,

$$\begin{aligned} h_0(x, z) &= \left[-s_1(z) \left(\frac{x}{\sigma_0} \right) + i \frac{s_3(z)}{12} \left(\frac{x}{\sigma_0} \right)^3 \right] r_3 \\ &+ \left[-i \frac{3s_4^2(z)s_5(z)}{8} + \frac{3s_4^3(z)s_6(z)}{16} \left(\frac{x}{\sigma_0} \right)^2 + i \frac{s_4^4(z)s_7(z)}{64} \left(\frac{x}{\sigma_0} \right)^4 \right] r_4, \\ h_1(x, z) &= \left[-s_1(z) + i \frac{s_2(z)}{4} \left(\frac{x}{\sigma_0} \right)^2 \right] r_3 - \left[\frac{3s_4^3(z)s_5(z)}{4} \left(\frac{x}{\sigma_0} \right) + i \frac{s_4^4(z)s_6(z)}{16} \left(\frac{x}{\sigma_0} \right)^3 \right] r_4, \\ h_2(x, z) &= i \frac{s_2(z)}{4} \left(\frac{x}{\sigma_0} \right) r_3 + \left[\frac{3s_4^3(z)s_6(z)}{16} + i \frac{3s_4^4(z)s_5(z)}{16} \left(\frac{x}{\sigma_0} \right)^2 \right] r_4, \\ h_3(x, z) &= i \frac{s_3(z)}{12} r_3 - i \frac{s_4^4(z)s_6(z)}{16} \left(\frac{x}{\sigma_0} \right) r_4, \\ h_4(x, z) &= i \frac{s_4^4(z)s_7(z)}{64} r_4, \end{aligned} \quad (9)$$

where $r_3 = k_3 \sigma_0 / (6k_1)$ and $r_4 = k_4 \sigma_0^2 / (24k_1)$ with $\sigma_0^2 = \epsilon / (2\sqrt{k_1})$. As noted in Ref. [4], r_3 and r_4 are the perturbation parameters. The functions $s_i(z)$ are given by

$$\begin{aligned} s_1(z) &= \tan^2(\sqrt{k_1} z / 2), \\ s_2(z) &= \sec^2(\sqrt{k_1} z / 2) \tan(\sqrt{k_1} z / 2), \\ s_3(z) &= (2 + \sec^2(\sqrt{k_1} z / 2)) \tan(\sqrt{k_1} z / 2), \\ s_4(z) &= \csc(\sqrt{k_1} z), \\ s_5(z) &= 4\sqrt{k_1} z + 2\sqrt{k_1} z \cos(2\sqrt{k_1} z) - 3 \sin(2\sqrt{k_1} z), \\ s_6(z) &= 12\sqrt{k_1} z \cos(\sqrt{k_1} z) - 9 \sin(\sqrt{k_1} z) - \sin(3\sqrt{k_1} z), \\ s_7(z) &= 12\sqrt{k_1} z - 8 \sin(2\sqrt{k_1} z) + \sin(4\sqrt{k_1} z). \end{aligned} \quad (10)$$

The corresponding functions $g_i(x, z)$ for a defocusing case can be obtained by replacing the trigonometric functions in $h_i(x, z)$ with the corresponding hyperbolic functions. For a drift space, the unperturbed kernel is enough to get the final wave function:

$$K_0^{(0)}(x_2, z; x_1, 0) = \left(\frac{1}{2\pi i \epsilon L} \right)^{1/2} e^{\frac{i}{2\epsilon z} (x_2 - x_1)^2}. \quad (11)$$

where z is the length of the drift space.

Because the beam wave function includes some perturbed terms after passing a quadrupole magnet with aberration, we generalize the initial beam wave function like

$$\psi_1(x, 0) = \left(\frac{1}{2\pi\sigma_1^2} \right)^{\frac{1}{4}} \exp \left[-\frac{x^2}{4\sigma_1^2} + i \left(\frac{x^2}{2\epsilon\rho_1} + \theta_1 \right) \right] \left\{ 1 + \sum_{n=0}^4 a_n \left(\frac{x}{\sigma_0} \right)^n \right\} \quad (12)$$

where $a_n = \mathcal{O}(k_3, k_4)$ describes the perturbation effects.

After a drift space, the wave function becomes

$$\begin{aligned} \psi_2(x, z) &= \int dx_1 K_0^{(0)}(x, z; x_1, 0) \psi_1(x_1, 0) \\ &= \left(\frac{1}{2\pi\sigma_2^2} \right)^{\frac{1}{4}} \exp \left[-\frac{x^2}{4\sigma_2^2} + i \left(\frac{x^2}{2\epsilon\rho_2} + \theta_1 + \theta_2 \right) \right] \left\{ 1 + \sum_{n=0}^4 a_n \left(\frac{\sqrt{2}\sigma_1}{\sigma_0} \right)^n I_n \left(\frac{x}{\sqrt{2}\sigma_2}, \theta_2 \right) \right\}, \end{aligned} \quad (13)$$

where the parameters θ_2, σ_2 , and ρ_2 after the drift space are related to the corresponding initial parameters θ_1, σ_1 , and ρ_1 . The explicit formula can be found in Ref. [5]. The functions $I_n(x, \theta)$ in the final wave function are given by

$$\begin{aligned} I_0(x, \theta) &= 1, \quad I_1(x, \theta) = \frac{1}{2} e^{2i\theta} H_1(x), \quad I_2(x, \theta) = \frac{1}{4} e^{4i\theta} H_2(x) + \frac{1}{2}, \\ I_3(x, \theta) &= \frac{1}{8} e^{6i\theta} H_3(x) + \frac{3}{4} e^{2i\theta} H_1(x), \quad I_4(x, \theta) = \frac{1}{16} e^{8i\theta} H_4(x) + \frac{3}{4} e^{4i\theta} H_2(x) + \frac{3}{4}, \end{aligned} \quad (14)$$

where $H_n(x)$ are the Hermite polynomials.

After a focusing lens of the effective length of z , the wave function becomes

$$\begin{aligned} \psi_2(x, z) &= \int dx_1 K_f(x, z; x_1, 0) \psi_1(x_1, 0) \\ &= \left(\frac{1}{2\pi\sigma_2^2} \right)^{\frac{1}{4}} \exp \left[-\frac{x^2}{4\sigma_2^2} + i \left(\frac{x^2}{2\epsilon\rho_2} + \theta_1 + \theta_2 \right) \right] \left\{ 1 + \sum_{n=0}^4 (h_n + a_n) \left(\frac{\sqrt{2}\sigma_1}{\sigma_0} \right)^n I_n \left(\frac{x}{\sqrt{2}\sigma_2}, \theta_2 \right) \right\} \end{aligned} \quad (15)$$

For a defocusing case, the function h_n is replaced with g_n . The initial and final parameters, θ_i, σ_i , and ρ_i , can be obtained by the same formula as given in Ref. [5].

We note that the relation between initial model parameters, σ_1 and ρ_1 , and resulting parameters, σ_2 and ρ_2 , can be obtained by a well-known transformation of the twiss parameters [8],

$$\begin{pmatrix} \beta_2 \\ \alpha_2 \\ \gamma_2 \end{pmatrix} = \begin{pmatrix} R_{11}^2 & -2R_{11}R_{12} & R_{12}^2 \\ -R_{11}R_{21} & 1 + 2R_{12}R_{21} & -R_{12}R_{22} \\ R_{21}^2 & -2R_{21}R_{22} & R_{22}^2 \end{pmatrix} \begin{pmatrix} \beta_1 \\ \alpha_1 \\ \gamma_1 \end{pmatrix} \quad (16)$$

with $\gamma_i\beta_i - \alpha_i^2 = 1$. The twiss parameters are related to the TWM parameters through $\sigma_i = \sqrt{\epsilon_{\text{rms}}\beta_i}$ and $\rho_i = -\beta_i/\alpha_i$.

We also note that the final wave function is not normalized to one even though the initial wave function is normalized to be one. The reason is that the modulus squared of the wave function includes the second-order terms which are proportional to $\mathcal{O}(k_3^2, k_4^2)$. Because the particle distribution function becomes negative in some region if we keep the linear terms only in modulus squared, we have to use a modulus squared for the particle distribution.

Hence the normalization increase should be an indicator to evaluate the validity of the perturbation calculation. We found that normalization increases less than few percent from one, the perturbation calculation described the PARMILA calculation successfully.

In order to check the perturbation calculation, we compared the results with the PARMILA simulation with 50,000 macro particles which pass through a FODO lattice. The field gradient and the effective length of a quadrupole magnet are 10 T/m and 0.2 m, respectively. The length of a drift space is 0.5 m. In the simulation, we assumed that the field strengths of the sextupole and octupole components are 3% of the quadrupole strength. We used matched input beam of the lattice with the twiss parameters, $\alpha = -1.60$, $\beta = 2.37$ mm/mrad, and $\epsilon_{\text{rms}} = 1.56 \pi$ mm-mrad. They correspond to $\sigma_1 = 1.92$ mm and $\rho_1 = 1.48$ m. We used a Gaussian input beam and neglected the space charge effects.

Figure 1 shows the input particle distribution (histogram) for the PARMILA calculation and the model result (solid line). The input beam wave function is normalized to one in the mks unit. The particle distributions after each beam-optical component are given in from Figure 2 to Figure 5. The solid lines in figures show the TWM result with sextupole and octupole perturbations. We also included the pure quadrupole result as dotted lines in the figures to evaluate the validity of the results with and without aberration effects. The PARMILA calculation shows clearly that particle distribution deviates from a Gaussian distribution. The TWM with aberration successfully described the asymmetric result as shown in the figures. In order to compare the results quantitatively, we calculated χ values in each step. The result is summarized in Table 1. It shows that the TWM with aberration improves the result than the model without perturbation.

This work is related to the TWM calculation for a transverse beam dynamics of the charged particle with a sextupole and octupole perturbations. This model calculation is valid if space charge effects are negligible. Even though the perturbation result is limited to the first-order, it explained the PARMILA simulation results successfully when the aberration field strength is less than few percent of the quadrupole strength.

ACKNOWLEDGEMENTS

This work was supported by the Ministry of Education, Science, and Technology of the Korean government.

References

- [1] R. Fedele and G. Miele, *Nuovo Cimento D* 13 (1991) 1527.
- [2] R. Fedele and G. Miele, *Phys. Rev. A* 46 (1992) 6634.
- [3] S. A. Khan and M. Pusterla, *Eur. Phys. J. A* 7 (2000) 583.
- [4] R. Fedele, F. Galluccio and G. Miele, *Phys. Lett. A* 185 (1994) 93.
- [5] J. Jang, Y. Cho and H. Kwon, *Phys. Lett. A* 366 (2007) 246.
- [6] H. Takeda and J. Billen, PARMILA, LA-UR-98-4478.
- [7] H. Holstein, *Topics in Advanced Quantum Mechanics* (Addison-Wesley, 1992).
- [8] T. Wangler, *Principles of RF Linear Accelerators*, (John Wiley & Sons, 1998)

Table 1: χ values between PARMILA result and TWM calculation with and without aberration effects.

	initial	focusing quad.	1st drift	defocusing quad.	2nd drift
TWM without aberration	92.1	104.2	170.2	168.5	145.0
TWM with aberration	92.1	105.1	111.5	102.3	108.4

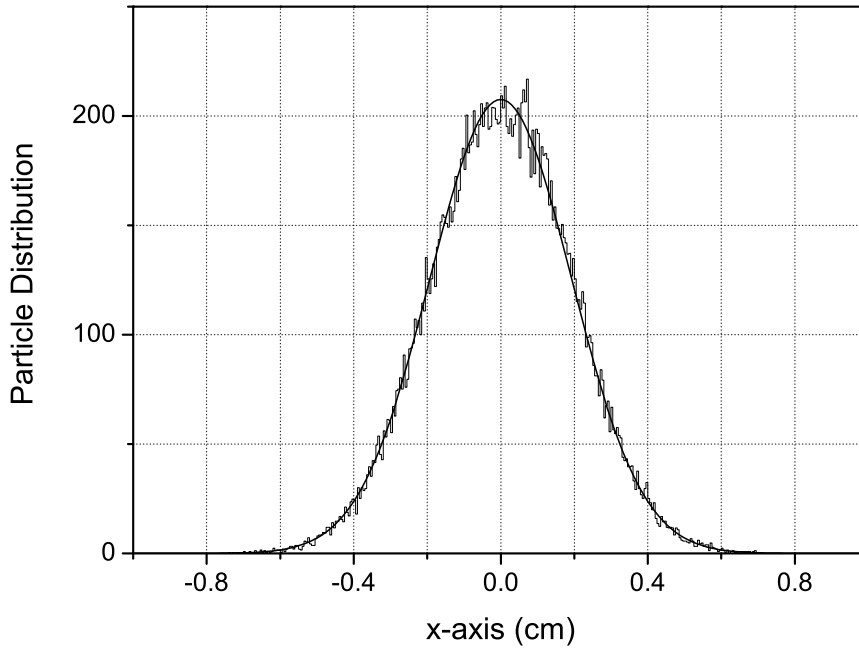


Figure 1: Particle distributions of the input beam. The histogram and solid line represent the PARMILA results and the model predictions, respectively.

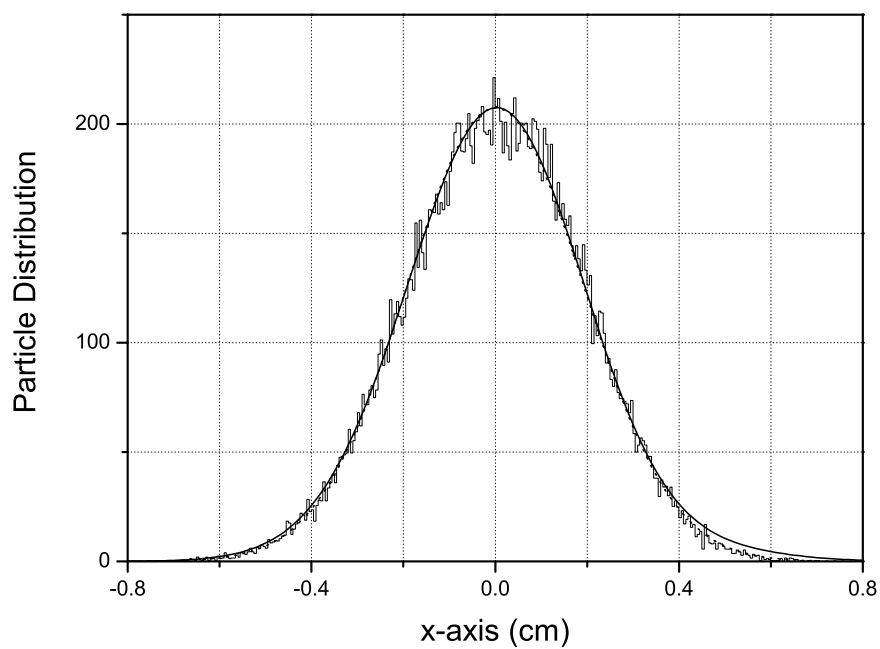


Figure 2: Particle distributions after the first quadrupole magnet. The histogram, solid, and dotted lines represent the PARMILA results and the model predictions with and without aberration, respectively.

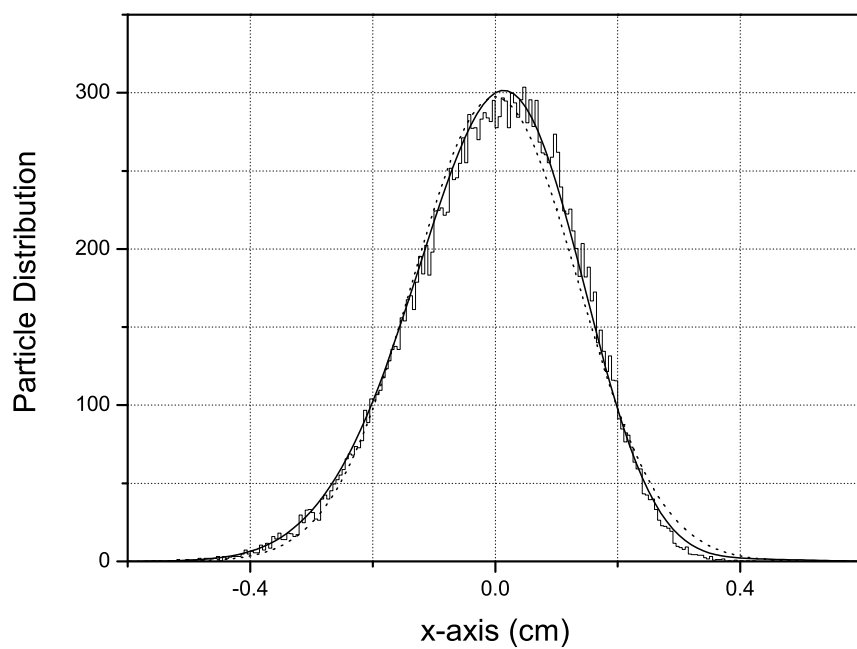


Figure 3: Particle distributions after the first drift space. The histogram, solid, and dotted lines represent the PARMILA results and the model predictions with and without aberration, respectively.

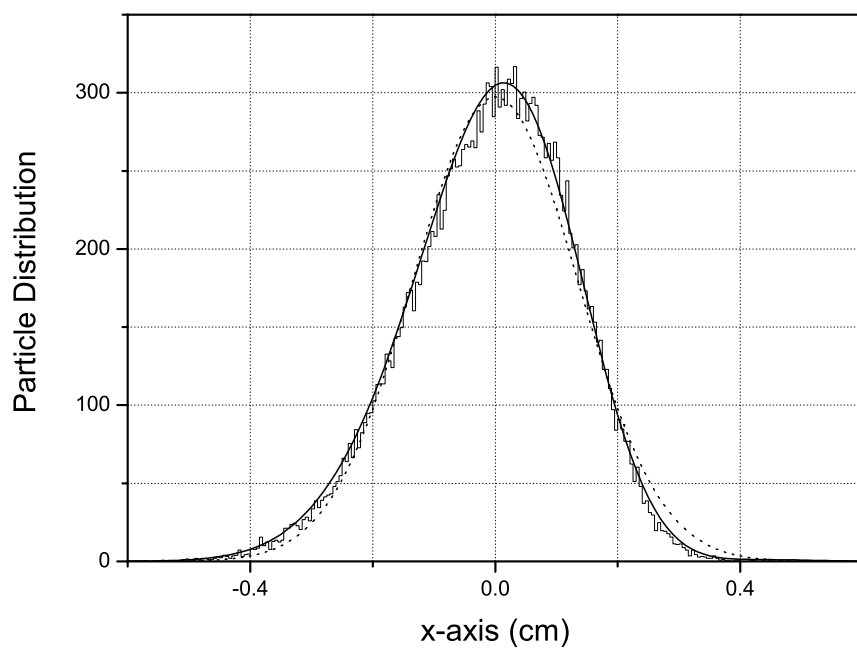


Figure 4: Particle distributions after the second quadrupole magnet. The histogram, solid, and dotted lines represent the PARMILA results and the model predictions with and without aberration, respectively.

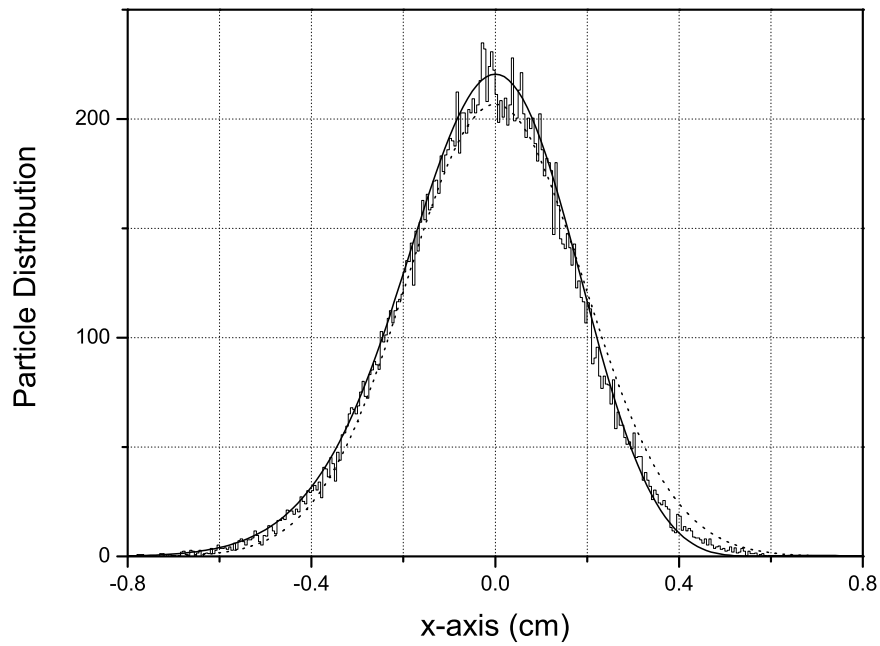


Figure 5: Particle distributions after the second drift space. The histogram, solid, and dotted lines represent the PARMILA results and the model predictions with and without aberration, respectively.